JOURNAL OF MATERIALS SCIENCE 22 (1987) 2309–2318

Delayed failure of a commercial vitreous bonded alumina

GEORGE D. QUINN
US Army Materials Technology Laboratory, Watertown, Massachusetts 02172, USA

The static fatigue resistance of a commercial low-cost alumina is evaluated. Flexural stress rupture results are compared to fracture mechanics crack growth testing. The original goal of this work was to develop satisfactory experimental procedures for the two test methods prior to more extensive testing on high-performance ceramics such as silicon nitride. The static fatigue trends measured by the two methods are comparable at 1000° C. The results are consistent with a model of static fatigue involving microcrack growth, coalescence and fracture due to stress corrosion. Creep deformations are very small, suggesting that creep fracture is not the mechanism of failure. A refined method for double torsion testing is presented.

1. Introduction

Considerable effort is being focused upon time-dependent failure of heat engine grade structural ceramics. Stress rupture and crack growth experimentation have attempted to detect and characterize static fatigue. Quinn [1] has reviewed the static fatigue of silicon carbides and nitrides. Stress rupture testing is commonly used to observe static fatigue phenomena. Tensile and flexural modes of loading have been used with the preponderance of data via the latter technique due to its relative experimental ease. Stress rupture tests require the application of a constant load to a sample. Analysis is straightforward and few assumptions are made. The major drawback is that considerable time may be required to conduct a test, which thereby limits data yield.

Alternative methods of obtaining data for static fatigue analysis include double torsion and dynamic strength testing. These methods either directly or indirectly measure growth rates of pre-existing flaws or large cracks. Fracture mechanics analysis can be used to relate the results to static fatigue. These tests are not foolproof methods of discerning static fatigue since they inherently measure only fast-moving cracks in specimens loaded nearly to fracture. Uncertainties in the crack growth functions and the need to extrapolate data render these alternative methods unreliable for the prediction of lifetimes in silicon nitride and carbide. Furthermore, these methods are only applicable to cases where failure occurs by the growth of pre-existing flaws or artificial cracks. Static fatigue can occur in other ways. Stress rupture testing, on the other hand, does not presume any mechanism of failure. Failure occurs by whatever mechanism is dominant for a given set of conditions.

In the 1970s and early 1980s, it was popular to attribute all static fatigue phenomena in high-performance ceramics to "slow crack growth". More recently, much attention has been focused on "creep fracture". These terms are not synonymous, and it is worthwhile to clarify some terms. The following nomenclature has been presented earlier [1], and is comparable to metallurgical interpretations.

"Static fatigue" is the most general expression applicable to failure of a specimen at a finite time after a load (often constant) is applied. "Stress corrosion", one possible mechanism of static fatigue, refers to the growth of cracks by chemical attack in stressed specimens. Stress corrosion may entail the nucleation of cracks as well. Environmental conditions are crucial. "Creep rupture" or "creep fracture" is an alternative mechanism, wherein bulk deformation causes the formation of extensive microcrack networks. These can coalesce to form larger cracks which eventually cause fracture. "Slow crack growth" is an expression which applies to the extension of a crack until it causes failure. It is usually used in the context of growth of pre-existing flaws as opposed to creep fracture (which entails nucleation and then growth). Furthermore, slow crack growth which may involve creep deformation and microcracking *local* to the crack tip, does not necessarily entail *bulk* creep and microcracking. It may not necessarily have an environmental dependence, thus distinguishing it from stress corrosion.

Crack growth and stress rupture data have been consistent in some instances, and very conflicting in others. For example, Quinn and Quinn [2] highlight an unsuccessful effort to correlate double torsion, flexural stress rupture and artificially flawed, flexural stress rupture data bases on a hot-pressed silicon nitride. The extreme inconsistency of published results on crack growth experiments was cited. One source of the difficulty is that more than one mechanism of time-dependent failure was operative in hot-pressed silicon nitride. The stress rupture experiments enabled the material to "choose" its method of failure, whereas double torsion experiments focused only upon the slow crack growth phenomenon.

Similarly mixed results were obtained in an effort to correlate strength (dynamic fatigue) and fracture mechanics techniques on five ceramic materials [3]. Consistent results were obtained on a low-expansion

0022–2461/87 $03.00 + .12

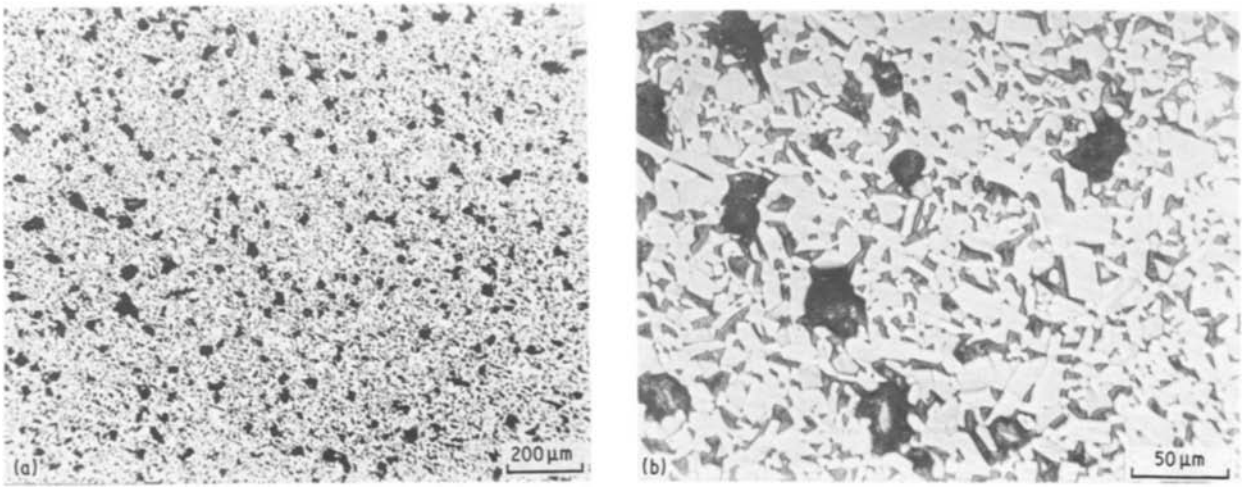

Figure 1 (a, b) Polished sections of AD-94 alumina showing the distributions of alumina (white), glass boundary phase (grey) and porosity (black).

glass and a glass–ceramic, but disagreement existed for another glass–ceramic and two grades of high-density aluminium oxide (Wesgo AL-300, 9 and 18 μm sizes). These mixed results were explained on the basis of microstructure. The coarser materials presumably had greater crack tip–microstructure interactions, which in turn led double torsion cracks to behave differently to small cracks in the strength experiments. Regions of differing crack growth resistance could also lead to variable behaviour [3].

In the last few years, it has become evident that a variety of factors can lead to conflicting life prediction parameters. These include material inhomogeneity, residual stresses, multiple mechanisms of static fatigue, new flaw generation, material chemistry or microstructural change with time, crack–microstructure interactions, multi-region stress intensity–crack velocity curve behaviour, redistribution of stress fields in flexure due to creep, and environmental factors. Inconsistent results by the same test method also indicate that most test methods have not been perfected and have significant experimental errors. This underscores the desirability of developing standard procedures.

The most reliable data for life prediction may come from stress rupture testing [1, 4]. Less extrapolation of the data is involved and the material is allowed to fail in static fatigue by whatever mechanism is dominant for a given stress, temperature and environment. Tensile testing is preferred, but most studies are based on flexure testing. Flexure testing is acceptable in many instances, but severe complications occur if non-linear creep deformation leads to stress redistribution.

The present report contains extensive results on a commercial alumina. Double torsion and flexural stress rupture experiments were performed at room and elevated temperatures. This work was performed in the late 1970s and early 1980s and is only now being published because of the resurgence of interest in the alumina family as model ceramics for the more expensive heat-engine materials. The original goal of this work was to develop experimental procedures as a precursor to more extensive study on hot-pressed silicon nitride [2]. A recent detailed study on a similar alumina (AD-96, Coors Porcelain Co.) emphasized the relation of static fatigue failure to creep deformation processes and grain boundary phase changes [5].

2. Material

AD-94 alumina (Coors Porcelain Co., Golden, Colorado) was chosen for the study. This grade is nominally 94% alumina and contains some glass and residual closed porosity. Inductively coupled plasma spectroscopy identified the following principal impurity elements (wt %): Si 1.9, Ca 0.63, Zr 0.55, Mg 0.47, Fe 0.10, Na 0.10 and Ni 0.08. Typical microstructures are shown in Fig. 1. The material has a mean crystallite size of 12 μm with a 2 to 25 μm range [6]. X-ray diffraction identified only alpha-alumina and an amorphous glass. No spinel was detected. The boundary phase glass in a similar alumina (AD-96, Coors Porcelain Co.) has been reported to be composed of silica and alumina with magnesium and sodium oxides as network modifiers [5]. Sonic modulus measurements gave an elastic modulus and Poisson's ratio of 291 GPa and 0.23, respectively. The bulk density of the material was 3.51 g cm^{-3}. These values are consistent with catalogue listings for this material [6]. The material was available in the form of tiles 152 mm × 152 mm square by 25.4 or 12.7 mm thick which were surplus from a study in the late 1960s to evaluate ballistic performance. A "C-scan" profile of one plate is shown in Fig. 2 which shows the variation in time of flight of a sound wave through the tile. The variations can be due to dimensional, density or elastic modulus changes. Fig. 2 illustrates the high uniformity of this material since the times-of-flight vary by only 1%. The alumina was chosen because it presumably could simulate a sintered high-performance ceramic with a glassy grain-boundary phase. The material was readily available, uniform and inexpensive to machine.

3. Experimental procedure

Several hundred flexure specimens were machined from a single billet of AD-94*. All specimens were

*Specimens from a different billet had significantly higher 1000° C fast-fracture strength due to a radically lower sodium content. This illustrates the importance of the refractoriness of the glassy phase and the need to keep careful track of billet-to-billet differences.

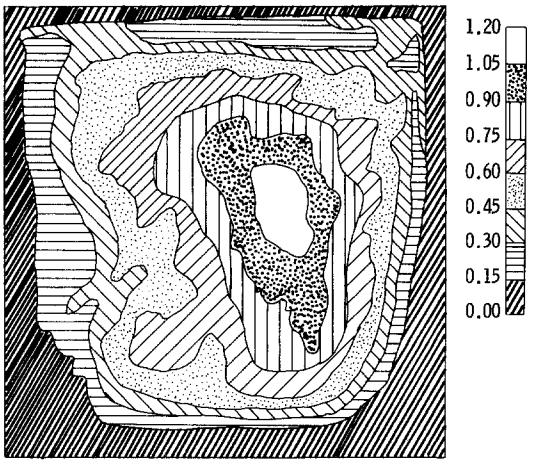

Figure 2 A C-scan profile of a 152 mm × 152 mm plate. The bar key on the right shows the percentage change in time of flight (increase) relative to the outer rim.

2.2 mm × 2.8 mm × 50 mm in size and were prepared with longitudinal surface grinding and 0.13 mm corner chamfers. Room temperature four-point flexure strength was determined with fixed bearing edge fixtures with 40.6 mm × 20.3 mm spans. A constant displacement rate universal testing machine (Instron Model TT-DL, Canton, Massachusetts) was used with a crosshead rate of 2.5 mm min^{-1}. Times to failure were approximately 3 sec. Relative humidity was 33 to 58%.

Flexural strength was determined at 1000° C in air with fixed bearing, four-point fixtures with 38.0 and 19.0 mm spans. Crosshead displacement was 1.3 mm min^{-1} which resulted in failure in about 6 sec.

Flexural stress rupture experiments were done in air at 1000° C with relative humidities between 20 and 80%. Fixed bearing spans of 38 and 19 mm were used. Experiments were from 3.6 sec to several thousand hours in duration. Applied stresses were computed on the basis of the elastic simple beam theory formulation. Additional details on the strength and stress rupture procedures are presented elsewhere [2, 7].

Double torsion (DT) experiments were done to directly measure crack growth rates at room temperature and 1000° C. The fixtures are shown in Fig. 3. The choice of fixture geometry was dictated by the furnaces used for the high-temperature testing. Since these furnaces had provision for loading from the top centre of the chamber, a lever beam on the DT fixtures was used. Half the load is transmitted to the two load pins at the front of the specimen, and the other half to the rear of the fixture base. This manner of loading and the large area of the fixture base serve to evenly distribute the load and reduce the bearing pressure on the firebrick below. One beneficial result of the design is that the load beam rests on three points and thus is self-aligning and does not tend to topple. This was helpful when specimens were loaded on to the fixtures inside heated furnaces. The fixtures were made of hot-pressed silicon carbide. Specimen size was 25 mm × 89 mm × 2.3 mm. A groove 2.5 mm wide was cut 0.76 mm deep down the centre of the specimen to encourage the crack to run straight. Subsequent to this study, it was determined that the groove is unnecessary.

The stress intensity factor for the DT sample is a function of applied load, specimen dimensions and Poisson's ratio, but not crack length:

$$K_I = PW_m \frac{3(1 + \nu)}{Wt^3 t_n} \quad (1)$$

where P is the applied load to the specimen, W is the specimen width, W_m is the moment arm, t is the specimen thickness, t_n is the thickness of the specimen at the notch and ν is Poisson's ratio. Plasticity would reduce the stress intensity at the crack tip, but an analysis indicates that the effect may be small [8]. No provision for the curved crack front was made.

Two methods of DT testing were used. The first method employed a constant displacement rate, universal testing machine (see earlier) to measure crack velocity via a load relaxation process that is slightly different to the usual reported procedure. A

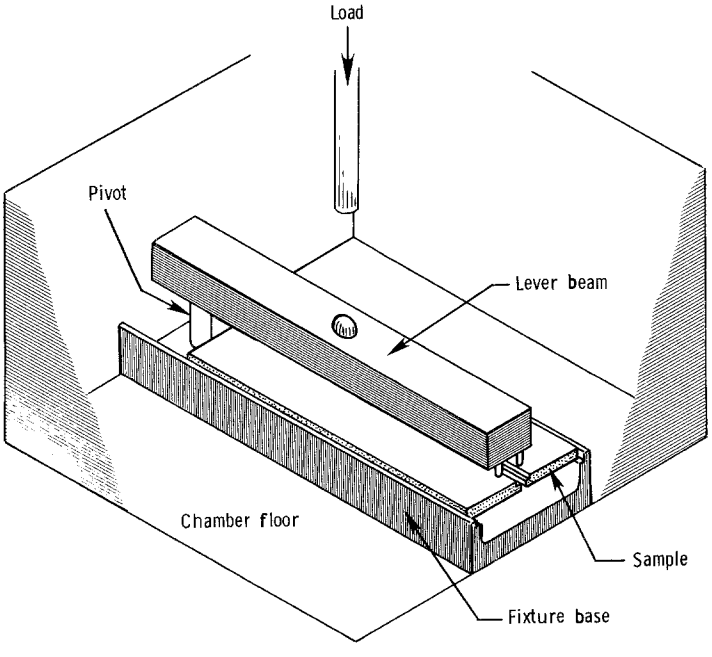

Figure 3 Double torsion fixtures. The specimen is loaded with the groove in the "compression" orientation.

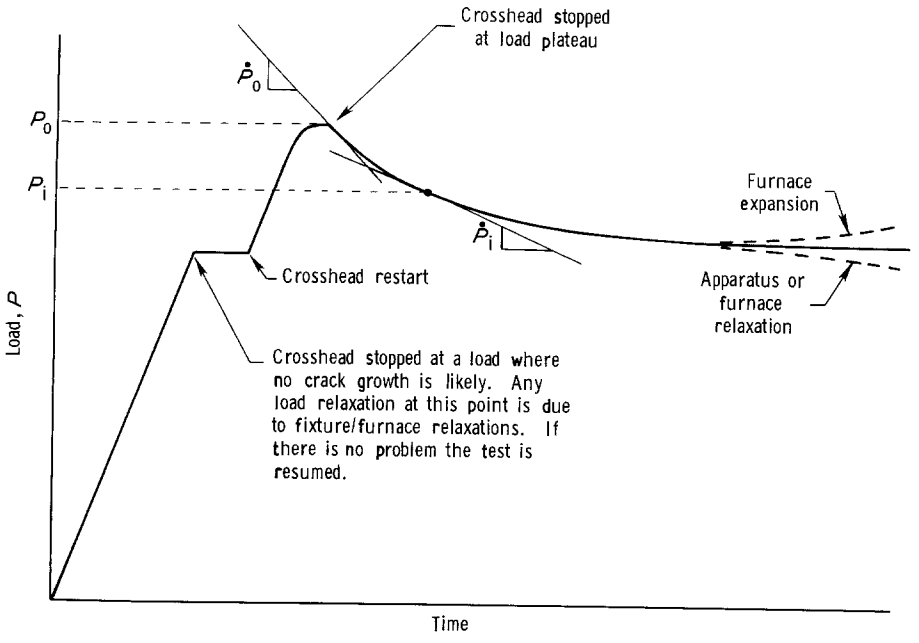

Figure 4 Load–time chart for a double torsion relaxation trial.

specimen was loaded at a constant displacement rate (not necessarily fast) until a load plateau occurred (Fig. 4) and the crosshead was immediately stopped. At this point

$$\dot{P} = \mathrm{d}P/\mathrm{d}t = 0 \quad (2)$$

A load relaxation curve results since the crack is still moving although decelerating. Eventually the crack will arrest and the load will remain constant. The crack velocity at any instant of time during this relaxation process can be shown to be [9]

$$V = \left(\frac{\dot{y}}{B}\right)\left(\frac{P_0}{\dot{P}_0}\right)\left(\frac{\dot{P}_i}{P_i^2}\right) \quad (3)$$

where $\dot{y}$ is the rate of crosshead motion during the loading, and P_0, $\dot{P}_0$, P_i and $\dot{P}_i$ are loads and load relaxations defined in Fig. 4. B is a specimen compliance term given by

$$B = \frac{3W_m^2}{Wt^3G}$$

Shear moduli (G) of 118 and 110 GPa were used for room temperature and 1000° C, respectively. The room temperature value was computed from the elastic modulus and Poisson's ratio. The 1000° C value is an estimate based upon a projected decrease of G with temperature [10]. Crosshead speeds of 0.05 and 0.13 mm min^{-1} were used for the room temperature and 1000° C experiments, respectively.

Advantages of this DT relaxation approach include: precracking can occur during a test; crack lengths need not be measured; and there are no assumptions regarding the amount of fixture elastic compliance relative to specimen compliance. It *is* necessary to ensure that all relaxations are in the specimen and the apparatus itself does not relax. This is difficult to achieve in high-temperature furnaces. Care was taken in this study to eliminate such extraneous relaxations. In particular, it was helpful to overload the fixtures, with a dummy specimen in place, by a factor of two for one hour while at operating temperature. The elimination of extraneous relaxations was verified on each test by stopping the crosshead during the initial loading (Fig. 4). It is also necessary to ensure that the furnace was not expanding or contracting. In practice, the specimen was loaded into the furnace after the furnace temperature and expansion had stabilized overnight. In this study minimum crack velocities of the order of 10^{-6} m sec^{-1} were measured by this technique. Expanded load scales were used on the universal testing machine in order to magnify the load relaxation curves.

The second DT method used dead-weight loading in a stress rupture furnace. Crack velocities were calculated by measuring the initial and final crack position and dividing the difference by the elapsed time. In this process, no assumptions regarding system or specimen compliance are involved. In fact, the only assumptions are that the crack velocity is constant during the interval the crack front is straight, and that negligible growth occurs during loading and unloading.

Each specimen was loaded into the hot furnace and five minutes was allowed (once operating temperature was restored) prior to loading to ensure temperature stability. The load was then applied in the same manner as in a stress rupture test. Once the loading sequence was completed the furnace was reopened and the specimen was extracted slowly (to avoid thermal stresses). Crack lengths were measured with dye penetrant (Spotcheck SKL-HF, Magnaflux Corp., Chicago, Illinois) and a binocular microscope at magnifications up to 100 ×. A change in crack length of 0.1 mm could be discerned. Velocities as low as 1×10^{-8} m sec^{-1} were measured. The longest duration experiment was 88 h. Multiple trials were performed on several specimens. Specimens were precracked at 1000° C using the universal testing machine.

Crack velocity data from either DT technique were used only when the cracks were at least one-half the width away from the ends of the specimen. Very little success was achieved with the specimen oriented with the notch down ("in tension"). The crack would usually run out of the groove and veer to the side. The

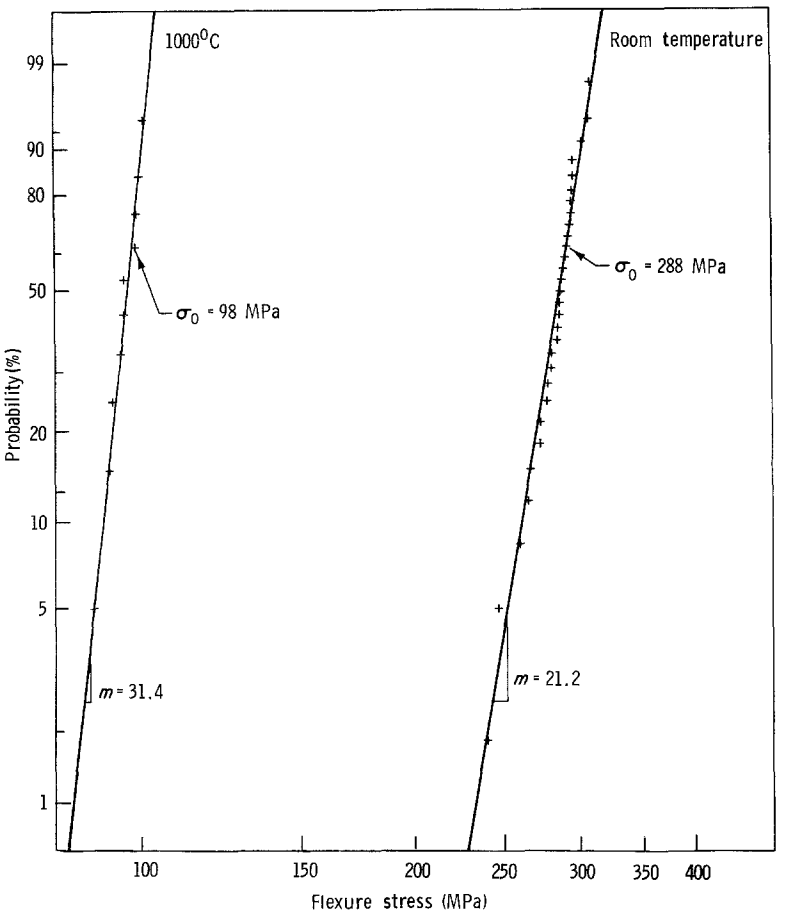

Figure 5 Weibull plot of room temperature and 1000° C strength of AD-94. The characteristic strength of the bend bar is labelled σ_0. At room temperature, stress values ranged from 238 to 306 MPa to give an average of 281 MPa and standard deviation 16 MPa. At 1000° C, values range from 90 to 101 MPa with an average of 97 MPa and standard deviations 3.7 MPa.

edges of the grooves acted as stress concentrators which attracted the crack. Results were much more successful when the specimen was oriented as shown in Fig. 3. It was determined at the end of this study that a key to successful DT testing, that is, getting a crack to pop-in and run straight, is alignment. Appendix I gives a recommended procedure, and a groove is completely unnecessary as verified by testing subsequent to this study.

4. Results

Fig. 5 gives the room-temperature reference strength of AD-94 alumina. The average strength, 281 MPa, is typical for a sintered alumina but the scatter is unusually low. The 1000° C average strength (Fig. 5) is considerably reduced to 97 MPa, but again the scatter is extremely low. Fractography was unfortunately not successful in identifying the strength-limiting defects. The microstructure was relatively coarse so that fracture mirrors were not evident. From the polished sections (Figs 1a and b) it may be inferred that the large, fairly uniformly dispersed, 40 to 50 μm sized pores could be strength-limiting.

Figs 6 and 7, and Tables I and II present the flexural stress rupture results. Thirty specimens each were used at 80, 70, and 60 MPa. Three 60 MPa specimens did not fracture and were terminated at times of 263, 263 and 1655 h. A 50 MPa specimen survived for 6455 h. Very little creep deformation (usually less than 0.1%) was noted in the specimens. Table I shows creep strains for several of the longer duration experiments. Final strains (greater than 0.05%) were determined by measuring the midspan deflection relative to the inner span from photographic enlargements*. Short-time strengths (90 MPa for 0.001 h) are consistent with the fast fracture strengths (90 to 100 MPa) at 1000° C (Fig. 5). The scatter in-times-to-failure is about one order of magnitude at 80 MPa, but increases dramatically at lower stresses. Careful attention was devoted to minimizing sources of experimental error and it is believed that the scatter is inherent to the material. A factor which certainly accounted for one unusually long time (6.5 h) for a 70 MPa specimen was that the specimen was inadvertently exposed to 1050° C for a few minutes prior to loading at 1000° C. This effect of a pre-heat treatment will be discussed later in more

TABLE I Flexural creep strains at 1000° C

Stress (MPa)	Failure time (h)	Creep strain (%)
70	10.5	0.06
70	135	0.14
70	487	0.05
70	420	0.18*
70	2666	0.12*
60	49.5	0.10
60	283	0.13
60	284	0.13
60	373	< 0.05
60	Survived 263	0.10
60	Survived 263	0.17
60	Survived 1665	0.31
50	Survived 6445	0.25

*Annealed 24 h, 1050° C.

*Strain = (4 × specimen thickness × midspan deflection)/(inner span)^2.

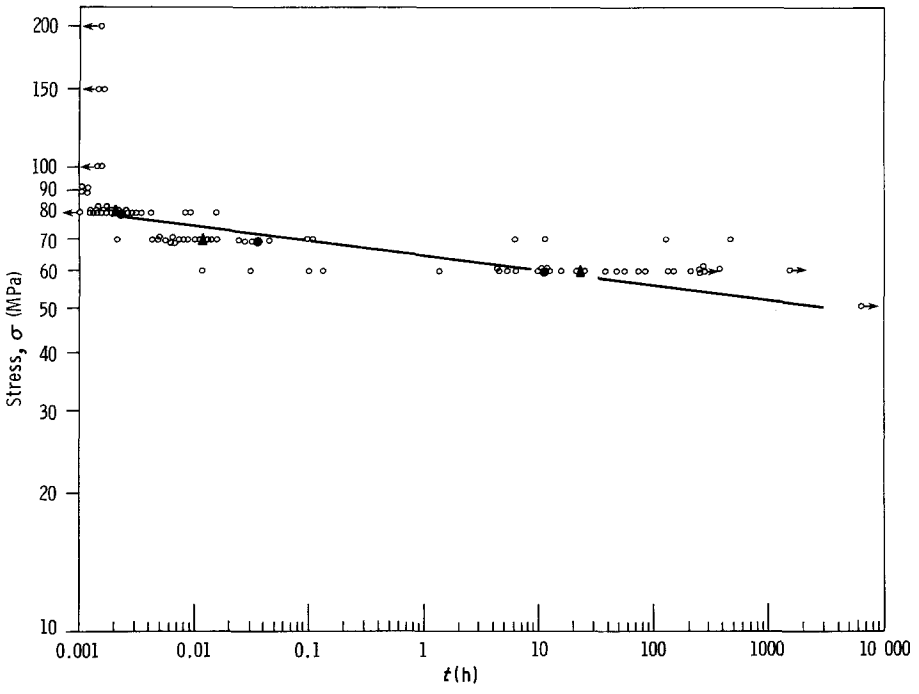

Figure 6 Flexural stress rupture of AD-94 at 1000° C in air on a log–log format. The line is a least-squares fitted line through the geometric mean times to failure at 80, 70 and 60 MPa. Points arrowed to the left were failures upon loading; arrowed to the right are specimens that survived intact. (▲) Medians, (●) geometric means. The line is represented by $\sigma = 64.4t^{-1/30.7}$.

detail. The few unusually long lifetimes at 70 MPa and short lifetimes at 60 MPa could not be correlated with abnormal humidity conditions.

The log–log representation (Fig. 6) appears to linearize the data better than the semi-log format (Fig. 7), but some curvature is evident. The line in Fig. 6 is a least-squares fitted line (using time as the independent variable) through the geometric *mean* times to failure at 80, 70 and 60 MPa. For comparison, the median values are shown as well. The outlier times to failure (long times at 70 MPa and short times at 60 MPa) account for the significant differences between the median and geometric mean except at 80 MPa where they coincide.

The regression fitted line of Fig. 6 implies

$$\text{flexure stress} = (64.4\,\text{MPa}) \times (\text{time})^{-1/30.7} \quad (4)$$

or

$$\text{time (h)} = (3.00 \times 10^{55}) \times (\text{flexure stress})^{-30.7} \quad (5)$$

The key parameter of interest here is the exponent, 30.7, which can be equated to the slow crack growth exponent N in the following empirical expression [11, 12]:

$$V = AK_I^N \quad (6)$$

where V is crack velocity, A and N are constants and K_I is the stress intensity.

The standard deviation of the exponent is estimated to be only 0.85 according to the analysis of Ritter *et al.* [12]. This low deviation implies a high precision, but it is dictated primarily by the high number of specimens tested for each of the three stresses, the high slow crack growth exponent, and the high Weibull modulus. The analysis does not consider the actual scatter in individual stress rupture outcomes. A more elaborate trivarient analysis is available [13] which may make more efficient use of the strength and fatigue data. The latter analysis makes certain assumptions which may not be met in this case and

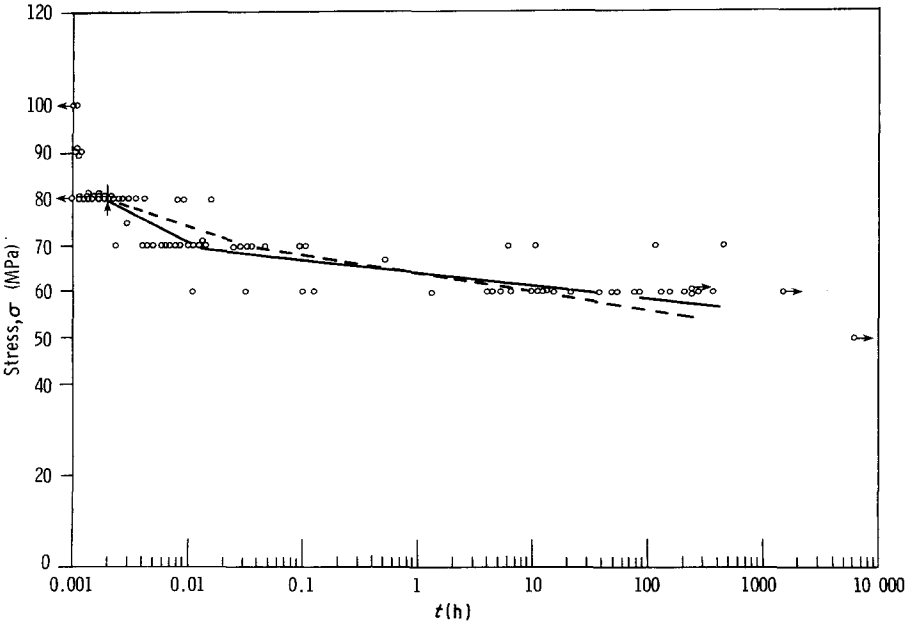

Figure 7 The same data as Fig. 6, but on a semilog format. The dotted lines connect the geometric means, the solid lines connect the medians.

TABLE II 1000° C stress rupture failure times, as-machined

Stress (MPa)		Failure times (h)
200		On Loading
150		Loading, Loading
100		Loading, 0.001
90		0.0007, 0.0007, 0.0009, 0.0010
80		0.0004, 0.0013, 0.0013, 0.0014, 0.0014, 0.0015, 0.0015, 0.0015, 0.0016, 0.0016, 0.0018, 0.0018, 0.0018, 0.0019, 0.0019, 0.0020, 0.0021, 0.0021, 0.0023, 0.0023, 0.0024, 0.0026, 0.0026, 0.0029, 0.0030, 0.0035, 0.0042, 0.0081, 0.0090, 0.0170
75		0.003
70		0.0024, 0.0041, 0.0047, 0.0048, 0.0049, 0.0058, 0.0064, 0.0064, 0.0067, 0.0069, 0.0075, 0.0080, 0.0081, 0.0100, 0.0106, 0.012, 0.014, 0.014, 0.016, 0.026, 0.028, 0.033, 0.035, 0.047, 0.098, 0.110, 6.2, 10.5, 135, 487
67		5.2
60		0.012, 0.031, 0.10, 0.13, 1.4, 4.4, 4.5, 5.2, 6.5, 10.0 10.9, 11.2, 11.4, 16.4, 21.2, 26.1, 39.2, 49.5, 53.4, 76.5, 83.4, 143, 154, 212, 283, 284, 373
	Survived	263, 263, 1665
50	Survived	6455

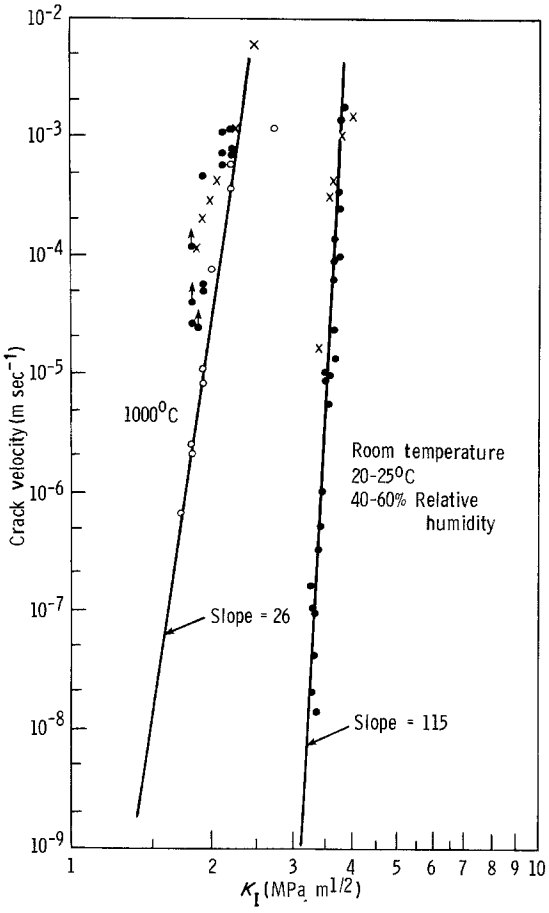

Figure 8 Double torsion crack velocity data at room temperature and 1000° C. The hollow circles at 1000° C are constant-load datum values for one especially well-behaved specimen. Arrowed points are best estimates, but could be as much as 50% too low. (x) Load relaxation, (●) dead-weight loading.

may not therefore be applicable, as will be discussed below.

The double-torsion crack velocity results are shown in Fig. 8. At room temperature, data from seven dead-weight loaded specimens were very consistent and in excellent agreement with load relaxation results on one other specimen. The five lowest velocities were obtained on three different specimens and correspond to crack advances of 0.5, 2.0, 3.5, 1.3, and 4.5 mm for times of 1.35, 5.5, 23.6, 18.0 and 88.0 h, respectively. The specimens did not exhibit a load history effect and datum values were reproducible despite interim experiments in different conditions. In only one instance, a crack apparently hit an obstacle and would not repropagate at the same K_I. It was necessary to apply a higher K_I to resume crack motion. The slow crack growth exponent, N, at room temperature was 115, which is in excellent agreement with values of 104 and 111 reported [3] for similar vitreous bonded aluminium oxides (two grades of Wesgo Al-300). The latter results were obtained with DT testing in distilled water.

Considerably greater scatter existed at 1000° C. In some instances, a specimen was loaded for times that should have caused reasonable crack extension, but the specimen fractured during the test. A lower limit to the velocity could be estimated as shown by the arrowed points in Fig. 8. In other cases, the crack apparently was pinned by some microstructural feature and required loading to a higher K_I to break free. The latter are not shown in Fig. 8. The load relaxation and dead-weight loading results overlap, but there may be a difference in apparent slopes. The fitted line through the 1000° C data was applied to dead-weight loading datum values on one especially consistent specimen. The lowest velocity determined came as a result of crack extension of 3 mm in 1.2 h. The slope of the line, the slow crack growth exponent N of Equation 6, is 26.

5. Discussion

A key issue is whether the double torsion and flexural stress rupture tests are measuring the same strength degradation due to static fatigue or even the same mechanism of static fatigue. The slow crack growth exponents N measured by the two methods at 1000° C in air are indeed quite similar, 26 and 31 respectively. This agreement must be tempered by the unsatisfying scatter in both data sets. Such scatter is not uncommon and every effort was made in this study to minimize experimental error. The higher scatter at 1000° C may be related to zones of variable chemistry or microstructure in this vitreous alumina material. Evidence to support this is that the double torsion fracture surfaces were rougher at 1000° C than at room temperature. Crack velocities varied considerably with position in a double torsion specimen, to the extent that with identical loadings, cracks grew to failure, or not at all in some instances. Slight variations in crack velocity can translate to large changes in lifetime. It can be plausibly argued that such zones of variable crack resistance should lead to differing

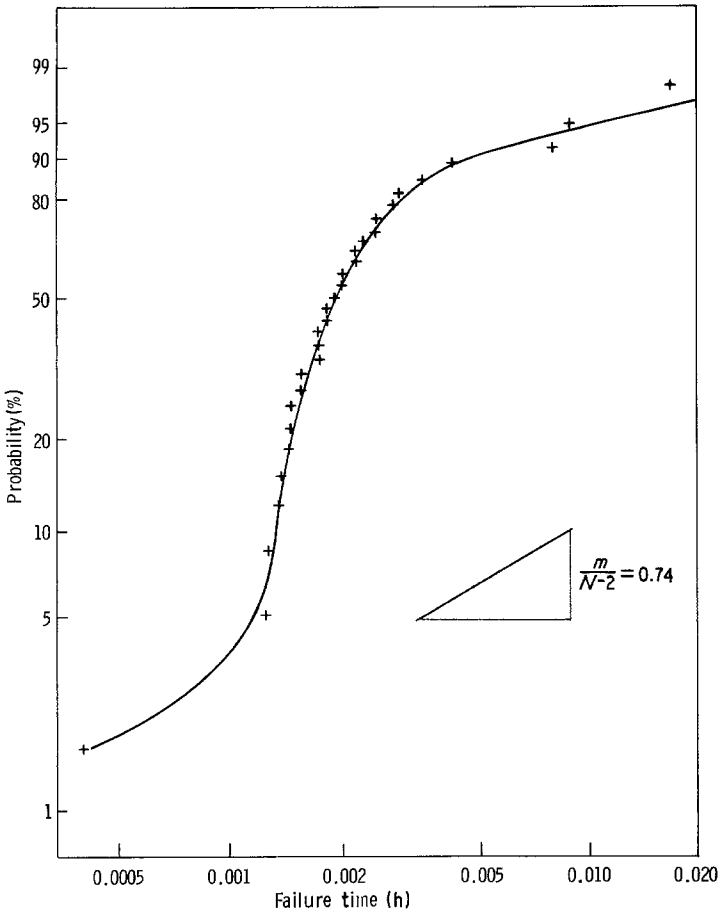

Figure 9 A Weibull cumulative probability of failure graph for the scatter in times to failure at 80 MPa in stress rupture at 1000° C. $P = (i - 0.5)/N$ for the ith datum.

results in strength against crack velocity experiments [3]. In that study, dynamic fatigue and crack velocity results did not agree for a similar alumina tested at room temperature.

The scatter in times-to-failure for 80 MPa stress rupture specimens is analysed in Fig. 9. The Weibull time distribution should be linear, with a slope of $m/(N - 2)$, if (i) fast fracture strengths fit a Weibull distribution (which Fig. 5 implies is true, both at room temperature and 1000° C); (ii) failure was due to slow crack growth from the same flaws which limit fast fracture strength; and (iii) slow crack growth can be represented by Equation 6 [11–14]. In this instance m is 21.2*, N is 30.7 for 1000° C and the slope should be 0.74. The failure of Fig. 9 to linearize the data implies that the above analysis is not applicable, which suggests that time-dependent failure was not due to slow crack growth from pre-existing flaws. A normal distribution did not adequately linearize the time data, nor did a normal distribution of log(times). The Weibull time distribution with the appropriate values of m or N did not fit the 70 or 60 MPa outcomes either†.

One common cause of disagreement in stress rupture against crack growth experiments is the different time regimes involved. This was not a problem in the present study. Stress rupture experiments are commonly conducted from 0.001 to 1000 h, whereas crack velocity experiments (such as load relaxation double torsion) are of the order of 0.001 to 0.1 h. Crack velocity experiments commonly measure velocities in the 1×10^{-2} to 1×10^{-6} m sec^{-1} range. Stress rupture experiments with natural flaws may involve velocities as low as 1×10^{-10} m sec^{-1}. The constant-load double torsion testing in this study extended results to comparably lower velocities and times. Indeed, a close examination of the 1000° C DT constant load results suggest an exponent somewhat different from one fitted through the relaxation data (Fig. 8). The reasonably long times of the constant-load DT experiments may contribute to the good agreement with the stress rupture data.

Although both the DT and the stress rupture/flexural strength data indicate a loss in load-carrying capacity at 1000° C relative to room temperature, the changes are different. The average flexural strength (a short duration test) changes from 281 to 97 MPa, a 65% drop. Fig. 8 suggests that the macrocrack critical stress intensity (K_{Ic}) changes considerably less. At 1×10^{-3} m sec^{-1} the stress intensity drop is only 39% from room temperature to 1000° C (3.75 to 2.29 MPa m$^{0.5}$).

As previously noted, one of the unusually long stress rupture lifetimes (70 MPa, 6.2 h) in the present study occurred for a specimen which was inadvertently exposed briefly to 1050° C prior to testing at 1000° C. To explore the possibility that this pre-exposure influences lifetime, an additional few experiments were conducted at 70 MPa, 1000° C on specimens deliberately annealed (no load) at 1050° C in air for either 1 or 24 h. The outcomes are shown in Fig. 10. Both

*The room temperature strength is used as an inert strength since loading times were short (~ 3 sec) and N is very high at room temperature (Fig. 8).

†There is of course a possibility that the time-to-failure distribution is a combination of the Weibull strength distribution and a material crack growth rate/spatial heterogeneity distribution, in which case analysis would be difficult.

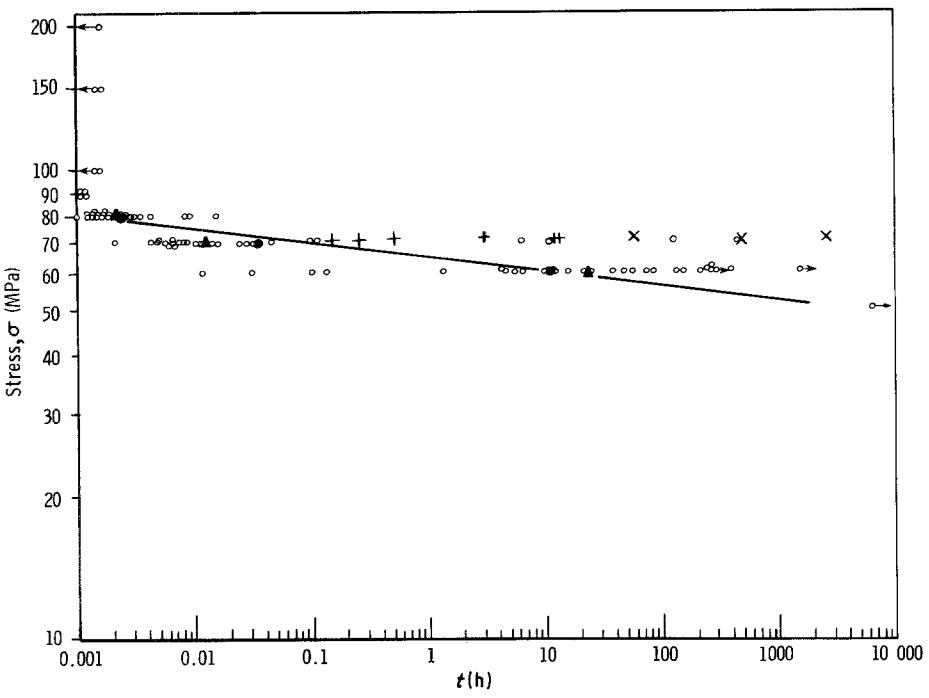

Figure 10 Flexural stress rupture of annealed specimens. (+) Annealed 1 h at 1050° C; (x) annealed 24 h at 1050° C. Other data points from Fig. 6.

treatments caused substantial increases in lifetime. It is conceivable that crack blunting, healing, or residual stress changes are operative. Most probably, recent evidence indicates that the glass grain boundary phase devitrifies as a result of a 1050° C exposure [5]. The partial devitrification leaves a more refractory glassy phase which has an increased viscosity and thus radically improved creep and stress rupture behaviour [5]. The observations in the present study reinforce these findings.

A recent study has suggested that stress rupture failure in a similar vitreous bonded alumina is due to creep fracture and not slow crack growth from pre-existing flaws at 980 to 1150° C [5]. This would be similar to the findings for hot-pressed silicon nitride under certain conditions [1, 15, 16]. The creep strains at failure observed in both reference [5] and the present report are very low however, usually less than 0.1%. This suggests that creep fracture was not the principal mechanism. Weiderhorn *et al.* [5] specifically reported that no evidence was found of cavitation; instead, extensive microcracked (delaminated) grain boundaries were common on the tensile surface. This observation will be referred to again.

In another study on a similar 96% alumina (Wesgo Al-300), it was reported that stress rupture failure at room temperature did not occur due to crack growth from a single worst flaw [17, 18]. Instead, failure was due to growth, interaction and coalescence of small grain-sized flaws after a small amount of intergranular crack growth. Microstructural heterogeneity and anisotropy controlled the local microcrack velocity. The mechanism of microcrack growth was assumed to be stress corrosion modelled by Equation 6. An analytical model was proposed wherein time-to-failure consisted of the sum of the time for microcracks to grow until coalescence while under local crack growth conditions, plus the time for coalesced cracks to grow to failure. A curious result is that the resultant equation for failure time, which integrates both micro- and macro-growth stages, still has the same stress dependency as Equation 5. Thus the stress exponent N for stress rupture failure due to micro-flaw growth, coalescence and failure will be the same as the stress intensity exponent for very large double torsion cracks. It should be emphasized that the experiments referred to [17, 18] were performed at room temperature and creep deformation was not a factor. It is believed that the same mechanism of failure can account for the stress rupture failures in the present study.

Fractographic examination of the stress rupture specimens should in principle clarify the issue of what mechanism is responsible for failure. Unfortunately, optical examination is difficult in this coarse-grained, porous, translucent, intergranularly cracking material. Sines and Okada [17, 18] reported similar difficulties which were overcome only by very careful dye penetration methods. Nevertheless, close examination of the tensile surfaces of long-duration stress rupture specimens in the present study revealed extensive microcrack networks, and the fracture surfaces were jagged and irregular. Either the creep fracture or alternatively the stress corrosion microcracking mechanisms would cause these features. As mentioned earlier, an important finding of Weiderhorn *et al.* [5] was that there was no evidence of cavitation. Thin grain-boundary "delaminations" were found instead. This fractographic finding lends credence to the stress corrosion microcracking model of failure and casts doubt upon the creep fracture model. In comparison, extensive creep damage and microcracking have been observed in hot-pressed silicon nitride, but only for specimens with high strains (0.3 to 2%) [15, 16].

In summary, there would appear to be several mechanisms of failure in coarse-grained, vitreous bonded aluminas. Fast fracture, both at room and elevated temperature, is probably controlled by the worst single flaw. Static fatigue can occur at high stresses and very short failure times by slow crack growth due to stress corrosion attack on the single worst flaw. At lower stresses and longer times, a microcrack growth, interaction coalescence and

fracture mechanism controls stress rupture failure from room temperature to 1000° C (or even higher). Finally, a creep fracture mechanism can cause stress rupture failures, but presumably only at high temperatures (above 1050° C) wherein creep processes lead to meaningful bulk deformations and cavitation. Extensive stress rupture testing would be necessary to define the stress–temperature–time regimes of each mechanism. Eventually these could culminate in fracture mechanism maps as have been presented earlier [15, 16, 19] for other materials.

6. Conclusions

The static fatigue resistance of a commercial vitreous bonded alumina was evaluated by double torsion and flexural stress rupture testing at room temperature and 1000° C in air. The static fatigue trends were comparable at 1000° C. Slow crack growth exponents were 25 and 31. This result is somewhat surprising in consideration of other published findings for ceramics wherein such agreement was not obtained. Local microstructural heterogeneities caused a large variation in times to failure and crack velocity results.

The similarities in static fatigue trends were consistent with a previously published model of microcrack growth, interaction, coalescence and fracture. The low bulk deformations observed implied that creep fracture was probably not a contributing mechanism at 1000° C (or below).

Annealing at 1050° C had a pronounced effect upon lifetime, confirming previously reported findings.

A refined method for double torsion testing was used successfully.

Acknowledgement

The author wishes to thank Dr S. Wiederhorn of the National Bureau of Standards for helpful discussions and encouragement to present the results.

Appendix: Double torsion preslitting procedure

Initial experimentation was hampered by a high incidence of crack curvature away from the centre axis of the specimen. The key to straight crack growth is straight and centred precracking and good alignment during the subsequent testing. A groove is unnecessary with these precautions.

The usual procedure is to preslit the specimen with a thin (0.25 mm) diamond cut-off wheel to a length at least one-half the specimen width. This preslitting can be done at a sharp angle as shown in Fig. A1. Such preslitting will often lead to the formation of small machining cracks at the slit tip, and it is these that usually pop-in and develop during the subsequent loading. Dye penetrant examination at 20× often reveals these machining cracks. If they are favourably oriented along the specimen long axis, then testing will be successful. If not, then once the large crack has popped in at an angle, nothing will prevent it from curving to the side. The remedy to this is to very carefully preslit to avoid the machining damage. A Knoop indenter can then be used to carefully scratch a one-centimetre line extending from the slit tip. The

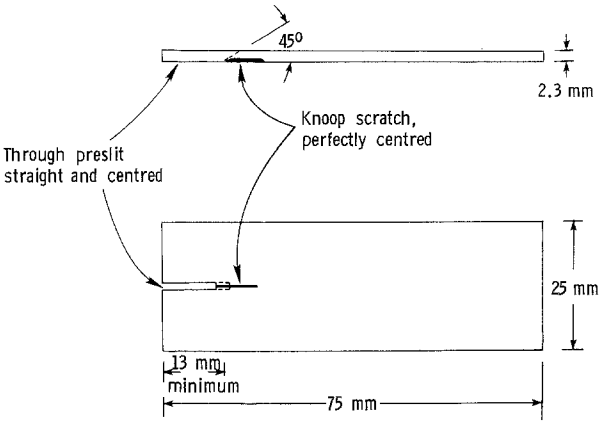

Figure A1 Preslitting procedure for a double torsion specimen. The depth of the Knoop scratch is exaggerated.

scratch should be very straight and centred on the specimen to within 0.1 mm. The preslit should also be as straight and centred as possible. The load to use on the Knoop indenter will vary with the material.

Precracking should be done with a hard universal testing machine. If the crack pops-in along the Knoop scratch and is straight, subsequent testing will be successful as long as the fixtures are well aligned.

References

1. G. QUINN, *Ceram. Eng. Sci. Proc.* **3** (1982) 77.
2. G. QUINN and J. QUINN, in "Fracture Mechanics of Ceramics 6", edited by R. Bradt, A. Evans, D. Hasselman and F. Lange (Plenum, New York, 1983) p. 603.
3. B. PLETKA and S. WIEDERHORN, *J. Mater. Sci.* **17** (1982) 1247.
4. S. WIEDERHORN and J. RITTER Jr, ASTM (American Society for Testing and Materials, Philadelphia, 1979) p. 202.
5. S. WIEDERHORN, B. HOCKEY, R. KRAUSE Jr and K. JAKUS, *J. Mater. Sci.* **21** (1986) 810.
6. "Coors Ceramics–Materials for Tough Jobs", Data Sheet FP5M (Coors Porcelain Co., Golden, Colorado, 1984).
7. G. QUINN, Technical Report TR 80-15 (Army Materials and Mechanics Research Center, Watertown, 1980).
8. A. EVANS and S. WIEDERHORN, *J. Mater. Sci.* **9** (1974) 270.
9. S. WIEDERHORN, in "Fracture Mechanics of Ceramics 2", edited by R. Bradt, D. Hasselman and F. Lange (Plenum, New York, 1974) p. 613.
10. "Engineering Property Data on Selected Ceramics, Volume III: Single Oxides", Report HB07 (Metal and Ceramics Information Center, Battelle Columbus Labs, Columbus, Ohio, 1981).
11. A. PALUZNY and P. NICHOLLS, in "Ceramics for High Performance Applications II", edited by J. Burke, E. Lenoe and R. Katz (Brook Hill, Chestnut Hill, Massachusetts, 1978) p. 95.
12. J. RITTER Jr, N. BANDYOPADHYAY and K. JAKUS, *Amer. Ceram. Soc. Bull.* **60** (1981) 798.
13. K. JAKUS, D. COYNE and J. RITTER Jr, *J. Mater. Sci.* **13** (1978) 2071.
14. J. HELFINSTINE, *J. Amer. Ceram. Soc.* **63** (1980) 113.
15. G. QUINN, ASTM (American Society for Testing and Materials, Philadelphia, 1984) p. 177.
16. *Idem, Ceram. Eng. Sci. Proc.* **5** (1984) 596.
17. G. SINES and T. OKADA, *J. Amer. Ceram. Soc.* **66** (1983) 228.
18. T. OKADA and G. SINES, *ibid.* **66** (1983) 719.
19. C. GANDHI and M. ASHBY, *Acta Metall.* **27** (1979) 1565.

Received 21 April
and accepted 11 November 1986